

The mechanism of ArF laser-induced fluorescence of dense plume matter – Electronic supplementary information

Xiaochun Wang ^a, Zhengyu Huang ^a, Po-Chun Chu ^a, Yue Cai ^{a,b},
Kelvin S.Y. Leung ^c, Judy T.S. Lum ^c, and Nai-Ho Cheung ^{a*}

^a Department of Physics, Hong Kong Baptist University, Kowloon Tong, Hong Kong,
China

^b ANA Artwork Material Analysis Ltd, Mong Kok, Hong Kong, China

^c Department of Chemistry, Hong Kong Baptist University, Kowloon Tong, Hong
Kong, China

Abstract

The published article reports a series of experiments that were designed to elucidate the mechanism of laser-induced fluorescence (LIF) of laser ablation plumes, or plume-LIF (PLIF) for short. Many of the arguments that support the main conclusions are technical. They include (1) LTE plasma assumptions, (2) PLIF signal lifetimes, (3) PLIF signal delays, (4) plume expansion modeling, and (5) photoabsorption bandwidths of dense plume matter. They are presented here in order to keep the article within reasonable length.

List of Figures

Fig.	Caption	Page
E1	Electron density based on the assumption that the Cu 515.3 nm line was broadened by Stark effect. Experimental conditions: The 355 and 193 nm laser fluences were 2.6 J/cm^2 and 190 mJ/cm^2 , respectively. Interpulse delay was 40 ns. Instrumental spectral resolution was 90 pm. Time was measured from the peak of the 355 nm pulse.	E5
E2	Plasma Boltzmann temperature. Experimental conditions identical to that of Figure S-1.	E6
E3	PLIF signal lifetime at various IPDs for the Cu 510.6 (top) and 515.3 (bottom) nm lines. Three ArF fluences were used, 230 mJ/cm^2 (black squares), 190 mJ/cm^2 (red circles), and 110 mJ/cm^2 (blue triangles). Error bars are based on the standard deviations of three or more trials.	E7
E4	Variation of the exponent β with time.	E10
E5	Plot of $\int_{t_i}^{t_f} I^2 dt$ against F for the ArF laser output. The integration limits t_i and t_f are chosen to completely bracket the ArF laser pulse. The best quadratic fit through the origin is also shown.	E12
E6	Plot of $\log \left(\int_{t_i}^{t_f} I^2 dt \right)$ against $\log (F)$ for the ArF laser output. The integration limits t_i and t_f are chosen to completely bracket the ArF laser pulse. The best linear fit is also shown.	E13

List of Tables

Table	Title	Page
E1	Interpulse and signal delay. The ArF fluence was 190 mJ/cm ² for brass and 33 mJ/cm ² for SnPb.	E8
E2	Photoabsorption bandwidth ΔW at four aluminum plume densities.	E11

LTE plasma assumptions

In the article, we argue that the plume emissions are not consistent with equilibrated plasma emissions. We will expand that argument below.

We will begin by assuming that the spectral emissions shown in Fig. 3 of the article are plasma emissions. We further assume that the Cu 515.3 nm line was Stark broadened so we can deduce the electron density n_e . We adopt Stark parameters for a plasma temperature of 10,000 K.¹ The electron density n_e so determined is shown in Fig. E1. As can be seen, for time t out to 140 ns, n_e is well above the threshold (10^{16} cm⁻³) for local thermal equilibrium (LTE).

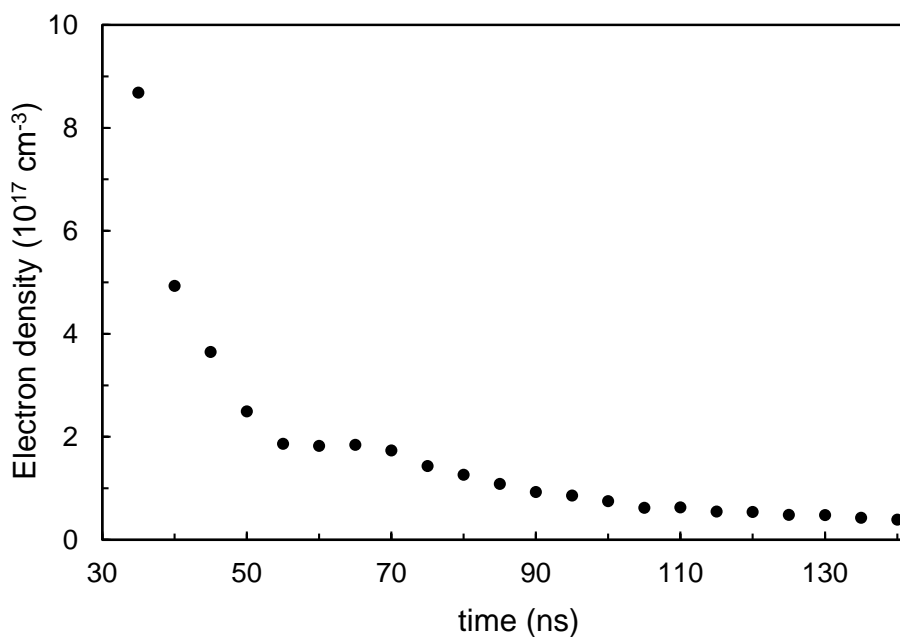


Fig. E1. Electron density based on the assumption that the Cu 515.3 nm line was broadened by Stark effect. Experimental conditions: The 355 and 193 nm laser fluences were 2.6 J/cm² and 190 mJ/cm², respectively. Interpulse delay was 40 ns. Instrumental spectral resolution was 90 pm. Time was measured from the peak of the 355 nm pulse.

We can therefore use the Boltzmann plot method to determine the plasma temperature T by using the intensity ratio of the Cu 510.6 and 515.3 nm lines.² The results are shown in Fig. E2. As can be seen, for t out to 140 ns, T is about 10,000 K or higher.

Based on Figs. E1 and E2, we can draw two conclusions. First, $T \sim 10,000$ K justifies our using Stark parameters for that temperature. Second, if the plume is truly an LTE plasma, there should be frequent enough electron collisions ($n_e > 10^{16}$ cm⁻³) at high enough kinetic energy ($T \sim 10,000$ K) to sustain the analyte emissions out to $t = 140$ ns. The fact that the analyte emissions were maximally enhanced at $t = 67$ ns and

then decayed promptly in the next tens of ns (see Fig. 3 of article) contradicts the LTE plasma assumption.

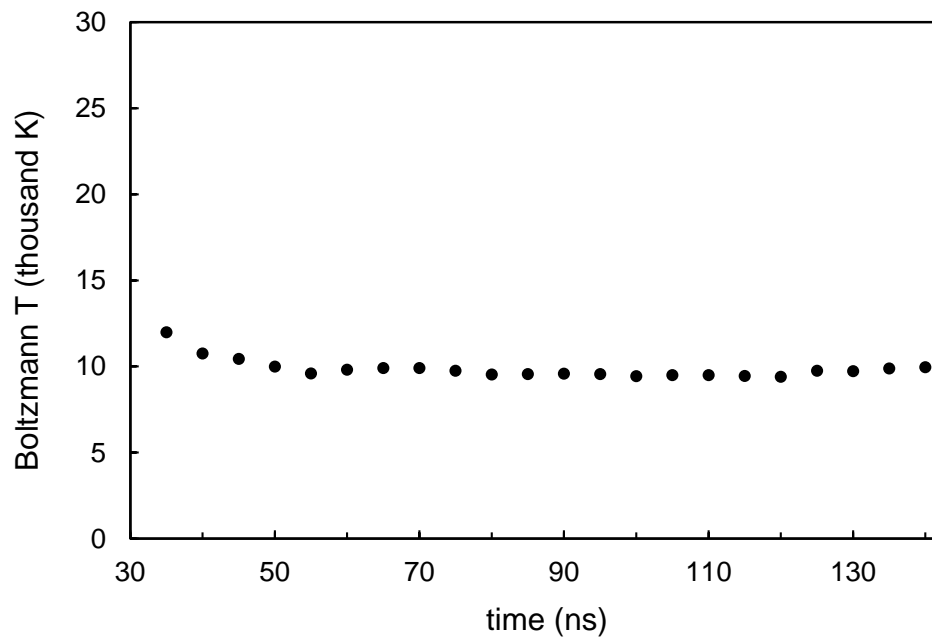


Fig. E2. Plasma Boltzmann temperature. Experimental conditions identical to that of Fig. E1.

PLIF signal lifetimes

In the article, we report the constancy of the lifetime of the PLIF signal regardless of the interpulse delay (IPD) and the ArF fluences. Fig. E3 is an illustration, where we plot lifetime against IPD for the Cu 510.6 and 515.3 nm lines at three different ArF fluences.

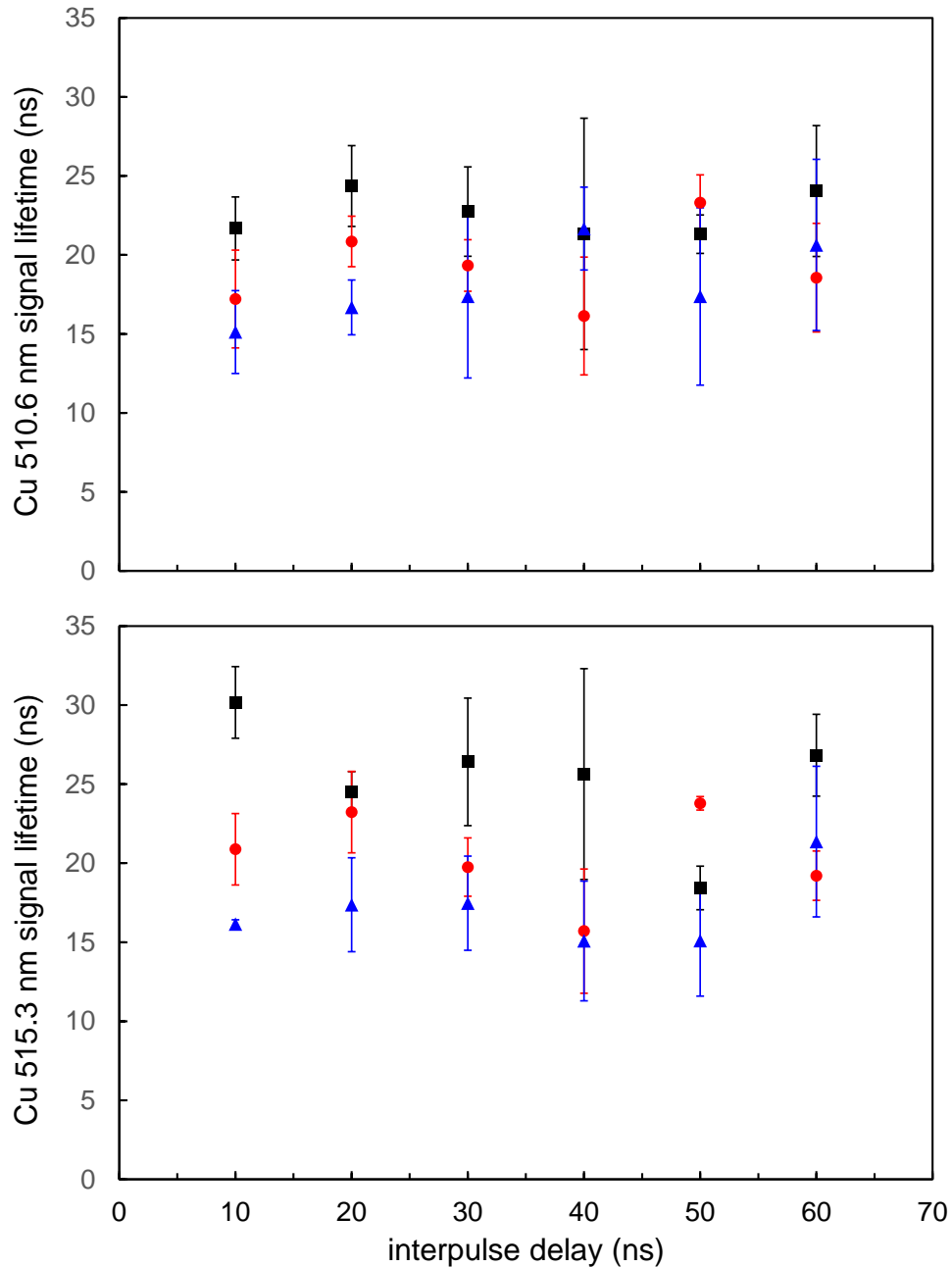


Fig. E3. PLIF signal lifetime at various IPDs for the Cu 510.6 (top) and 515.3 (bottom) nm lines. Three ArF fluences were used, 230 mJ/cm² (black squares), 190 mJ/cm² (red circles), and 110 mJ/cm² (blue triangles). Error bars are based on the standard deviations of three or more trials.

PLIF signal delays

We mention in the article that the PLIF signal was delayed from the ArF pulse. For instance, in Fig. 3 of the article, the PLIF signal peaked at about 67 ns which was 27 ns after the ArF pulse. This kind of signal delay was observed for a range of interpulse delay (IPD), and for both the brass and the SnPb targets. The delays are summarized in Table E1 below. Overall, the delay was 24 ± 3 ns for brass and 14 ± 4 ns for SnPb, regardless of IPD.

We speculate that the delay is due to the time needed for the photoexcited dense matter to morph into electronically excited analytes. See Section 3.4 of the article.

Table E1 Interpulse and signal delay. The ArF fluence was 190 mJ/cm^2 for brass and 33 mJ/cm^2 for SnPb

IPD (ns)		10	20	30	40	50	60	70	80	90	100
Signal	Brass	27.5	22.5	22.5	27.5	22.5	22.5	--	--	--	--
delay (ns)	Pb/Sn	17.5	22.5	17.5	12.5	12.5	12.5	12.5	7.5	12.5	12.5

Modeling plume expansion

We consider the expansion of a vapor plume that is produced by pulsed laser ablation. The expansion occurs in ambient air. We use the modified Sedov model to estimate the position of the plume front R as a function of time t (Ref. 3). $R(t)$ is given by,³

$$R(t) = R_o \left(\frac{t}{\tau} \right)^b,$$

where $\tau = 1$ ns is a convenient unit of time, and $b = \frac{2}{n+2}$ where n is the dimension of expansion. For our case of ns pulsed laser ablation at irradiance just below 1 GW/cm², the plume front initially propagates at about tens of km/s (Ref. 4) and R_o is therefore about tens of μm .

For $t < 10^1$ ns, the plume is expected to expand mainly along a direction normal to the target surface, i.e., approximately one-dimensionally.⁵ In our experiment, the crater radius is about tens of μm (12.5 –25 μm) which is about the same as R_o . The volume of the initial cylindrical plume can therefore be approximated by,

$$\begin{aligned} V &\approx \pi R_o^2 R_o \left(\frac{t}{\tau} \right)^{\frac{2}{3}} \\ &= \pi R_o^3 \left(\frac{t}{\tau} \right)^{\frac{2}{3}}. \end{aligned}$$

If N atoms are vaporized, the initial density will be given by,

$$\begin{aligned} \rho &= \frac{N}{V} \approx \frac{N}{\pi R_o^3} \left(\frac{\tau}{t} \right)^{\frac{2}{3}} \\ &= \rho_o \left(\frac{\tau}{t} \right)^{0.66}. \end{aligned}$$

where $\rho_o = \frac{N}{\pi R_o^3}$.

For $t > 10^1$ ns, the plume expansion will become more three dimensional.^{4,5} The position of the plume front R will be much greater than the crater radius. The volume of the hemispherical plume can therefore be approximated by,

$$\begin{aligned} V &= \frac{2}{3} \pi R^3, \\ &\approx \pi R_o^3 \left(\frac{t}{\tau} \right)^{\frac{6}{5}}, \end{aligned}$$

and the density is given by,

$$\rho \approx \rho_o \left(\frac{\tau}{t} \right)^{1.2}.$$

Generalizing, the plume density ρ decays with time t as,

$$\rho(t) \approx \rho_o \left(\frac{\tau}{t} \right)^\beta, \tag{E1}$$

where ρ_0 is the nascent density and the exponent β is 0.66, 1.0, and 1.2 for one, two, and three dimensional expansion, respectively.

We use Eq. (E1) to model $\rho(t)$. We define $t = 0$ to be the instant when the 355 nm irradiation is over and the vaporization of target material has completed. This is about 9 ns from the peaking of the 355 nm pulse. We set the initial plume density ρ_0 (ρ at $t = 1$ ns) to be $1.6 \times 10^{22} \text{ cm}^{-3}$ (Ref. 6). We allow the exponent β to vary with time t . At the earliest time of $t = 5.7$ ns that we modeled (14.7 ns from the peak of the 355 nm pulse), we set $\beta = 0.8$, i.e., almost linear. At the latest time of $t = 91$ ns that we modeled, we set $\beta = 1.2$, i.e., three-dimensional. We allow β to evolve gradually from 0.8 to 1.2 in between, as shown in Fig. E4. The result of our modeling is shown in Fig. 5(c) of the article when $\rho(t)$ is plotted in black.

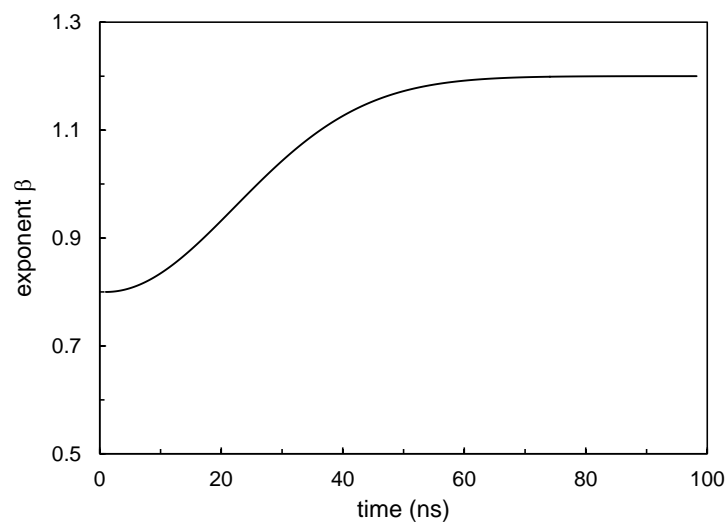


Fig. E4. Variation of the exponent β with time.

Photoabsorption bandwidth

We mention in the article that the photoabsorption bandwidth of the dense plume can be predicted once the plume density is known. The prediction is based on the dense-aluminum results computed by Mazevet *et al.* (2005).⁷ In Fig. 4 of Mazevet *et al.* (2005), the absorption coefficient α was plotted against photon energy E for a range of plume densities, in the form of a log-log plot. We curve-fitted the plot for E centering at 5.1 eV. We then replot $\alpha(E)$ using linear x and y scales, with x in terms of wavelength. The full-width-at-half-maximum ΔW of the 5.1 eV photoabsorption band is tabulated below for a range of plume densities. The last four entries are based on the results of Mazevet *et al.* (2005). The first three entries are artificial. They are introduced to ensure smooth curve-fitting at low density. A collisional width of 10 pm at 0.001 g/cm^3 ($2 \times 10^{19} \text{ cm}^{-3}$) is deemed reasonable.

Table E2 Photoabsorption bandwidth ΔW at four aluminum plume densities

Density σ (g/cm ³)	ΔW (nm)
0.001	0.01
0.002	0.02
0.003	0.03
0.025	4.25
0.1	14.9
0.3	140
0.5	450

We plot ΔW versus mass density σ and fit the trend with a fourth order polynomial, yielding,

$$\Delta W = -12,240\sigma^4 + 12,490\sigma^3 - 1,830\sigma^2 + 224\sigma - 0.41,$$

where ΔW is in nm and σ is in g/cm³. We can easily convert the mass density σ to number of aluminum atoms per volume ρ . So we can compute the absorption bandwidth in terms of the number density ρ of the plume. The results are shown in Fig. 5c (red curve) of the article.

Plotting $\int_{t_i}^{t_f} I^2 dt$ against F

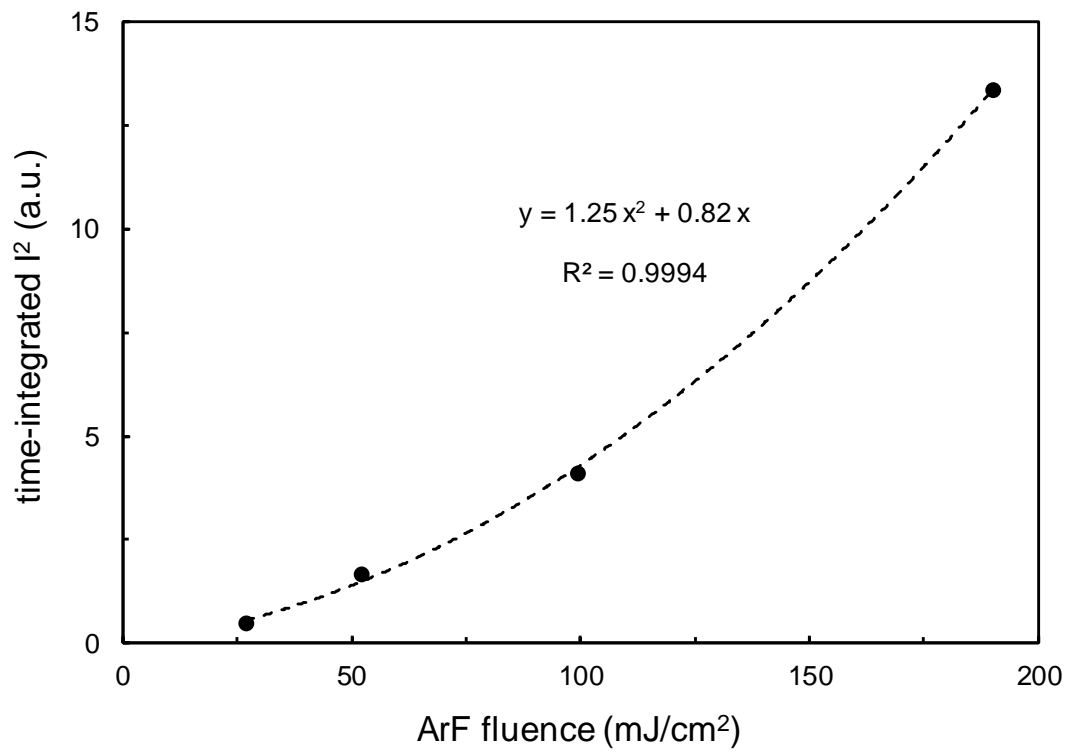


Fig. E5. Plot of $\int_{t_i}^{t_f} I^2 dt$ against F for the ArF laser output. The integration limits t_i and t_f are chosen to completely bracket the ArF laser pulse. The best quadratic fit through the origin is also shown.

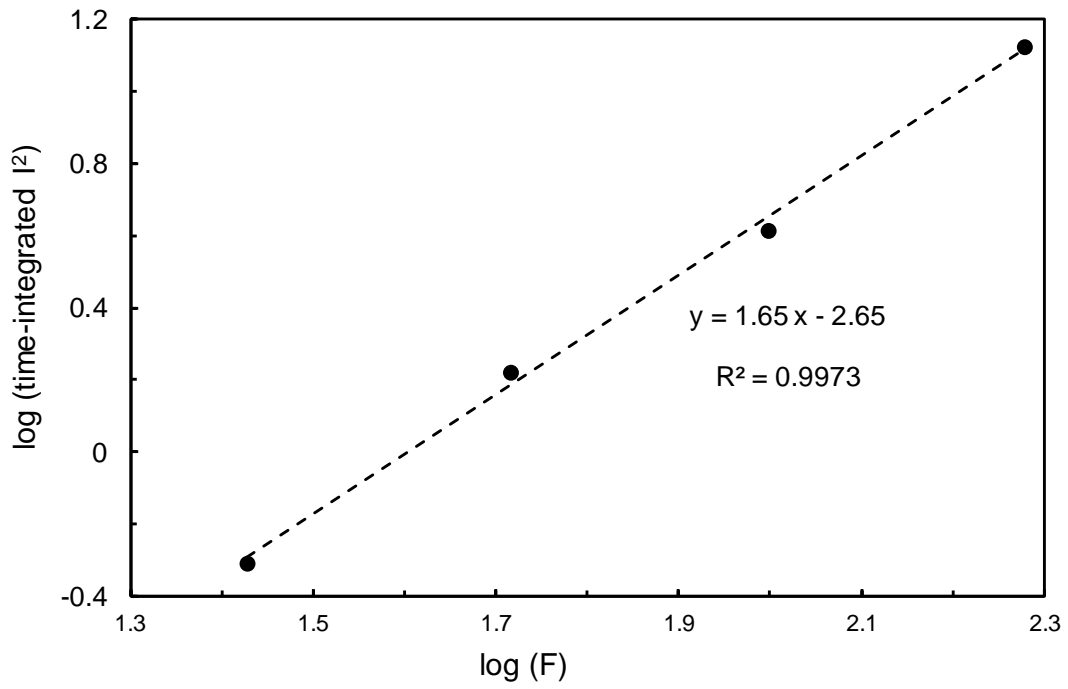


Fig. E6. Plot of $\log \left(\int_{t_i}^{t_f} I^2 dt \right)$ against $\log (F)$ for the ArF laser output. The integration limits t_i and t_f are chosen to completely bracket the ArF laser pulse. The best linear fit is also shown.

References

- 1 R.V. Semenyshyn, I.L. Babich, V.F. Boretskij, and A.N. Veklich, *Atomic data and Stark broadening of Cu I and Ag I spectral lines: Selection and analysis*. IX Serbian conference on Spectral line shapes in astrophysics, 2013.
- 2 H.R. Griem, *Principles of Plasma Spectroscopy*, Cambridge U Press: Cambridge, 2005.
- 3 S.S. Harilal, G.V. Miloshevsky, P.K. Diwakar, N.L. LaHaye, and A. Hassanein, *Phys. Plasmas*, 2012, **19**, 083504.
- 4 S.-B. Wen, X. Mao, R. Greif, R. and R.E. Russo, *J. Appl. Phys.* 2007, **101**, 023114.
- 5 C.R. Phipps, and R.W. Dreyfus, *The high laser irradiance regime*, in A. Vertes, R. Gijbels, and F. Adams, *Laser Ionization Mass Analysis*, Wiley-Interscience: New York, 1993.
- 6 D. Autrique, G. Clair, D. L’Hermite, V. Alexiades, A. Bogaerts, and B. Rethfeld, *J. Appl. Phys.* 2013, **114**, 023301.
- 7 S. Mazevet, M.P. Desjarlais, L.A. Collins, J.D. Kress, and N.H. Magee, *Phys. Rev. E*, 2005, **71**, 016409.